

Stopped-Flow Kinetics of Methyl Group Transfer between the Corrinoid-Iron-Sulfur Protein and Acetyl-Coenzyme A Synthase from *Clostridium thermoaceticum*

Xiang Shi Tan,[‡] Christopher Sewell,[‡] and Paul A. Lindahl^{*,‡,†}

Contribution from the Departments of Chemistry and of Biochemistry and Biophysics,
Texas A&M University, College Station, Texas 77843-3255

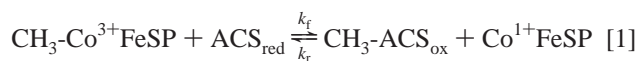
Received July 20, 2001

Abstract: Kinetics of methyl group transfer between the Ni–Fe–S-containing acetyl-CoA synthase (ACS) and the corrinoid protein (CoFeSP) from *Clostridium thermoaceticum* were investigated using the stopped-flow method at 390 nm. Rates of the reaction $\text{CH}_3\text{-Co}^{3+}\text{FeSP} + \text{ACS}_{\text{red}} \rightleftharpoons \text{Co}^{1+}\text{FeSP} + \text{CH}_3\text{-ACS}_{\text{ox}}$ in both forward and reverse directions were determined using various protein and reductant concentrations. Ti^{3+} -citrate, dithionite, and CO were used to reductively activate ACS (forming ACS_{red}). The simplest mechanism that adequately fit the data involved formation of a $[\text{CH}_3\text{-Co}^{3+}\text{FeSP}]:[\text{ACS}_{\text{red}}]$ complex, methyl group transfer (forming $[\text{Co}^{1+}\text{FeSP}]:[\text{CH}_3\text{-ACS}_{\text{ox}}]$), product dissociation (forming $\text{Co}^{1+}\text{FeSP} + \text{CH}_3\text{-ACS}_{\text{ox}}$), and CO binding yielding a nonproductive enzyme state ($\text{ACS}_{\text{red}} + \text{CO} \rightleftharpoons \text{ACS}_{\text{red}}\text{-CO}$). Best-fit rate constants were obtained. CO inhibited methyl group transfer by binding ACS_{red} in accordance with $K_D = 180 \pm 90 \mu\text{M}$. Fits were unimproved when >1 CO was assumed to bind. Ti^{3+} -citrate and dithionite inhibited the reverse methyl group transfer reaction, probably by reducing the D-site of $\text{CH}_3\text{-ACS}_{\text{ox}}$. This redox site is oxidized by $2e^-$ when the methyl cation is transferred from $\text{CH}_3\text{-Co}^{3+}\text{FeSP}$ to ACS_{red} , and is reduced during the reverse reaction. Best-fit K_D values for pre- and post-methyl-transfer complexes were 0.12 ± 0.06 and $0.3 \pm 0.2 \mu\text{M}$, respectively. Intracomplex methyl group transfer was reversible with $K_{\text{eq}} = 2.3 \pm 0.9$ ($k_f/k_r = 6.9 \text{ s}^{-1}/3.0 \text{ s}^{-1}$). The nucleophilicity of the $\{\text{Ni}^{2+}\text{D}_{\text{red}}\}$ unit appears comparable to that of Co^{1+} cobalamins. Reduction of the D-site may cause the Ni^{2+} of the A-cluster to behave like the Ni of an organometallic Ni^0 complex.

Introduction

Methyl group transfer reactions are involved in regulating gene expression and DNA replication, as well as in repairing genes, catabolizing nutrients, and synthesizing methionine.^{1–3} Methanogenic archaea and acetogenic bacteria use such reactions to synthesize methane and acetate.^{4–6} Methyl groups are typically transferred between organic and inorganic donors and acceptors, and commonly involve *S*-adenosylmethionine, methyl-tetrahydrofolate ($\text{CH}_3\text{-THF}$), cobalamins, and Ni porphyrins. The only such reaction thought to have both metal-ion donor and acceptor involves acetyl-coenzyme A synthases (ACS's).⁷ These $\{\text{Ni,Fe,Co,S}\}$ -enzymes are involved in the autotrophic

synthesis of acetyl-CoA using the Wood/Ljungdahl pathway.⁶ In *Clostridium thermoaceticum*, a corrinoid-Fe-S-containing protein (CoFeSP) exists independently of a Ni-Fe-S-containing ACS. During catalytic synthesis of acetyl-CoA, a methyl group is transferred from $\text{CH}_3\text{-Co}^{3+}\text{FeSP}$ to reduced ACS (ACS_{red}), reaction 1.



In this reaction, a methyl cation is transferred as the Co^{3+} cobalamin is reduced to Co^{1+} . The resulting $\text{CH}_3\text{-ACS}_{\text{ox}}$ is a stable catalytic intermediate capable of reacting with CO and CoA to yield acetyl-CoA (and ACS_{red}).^{8–10} ACS is a bifunctional enzyme that also catalyzes the reversible oxidation of CO to CO_2 at another active site.

The site within ACS that accepts the methyl group is a novel Ni-X- Fe_4S_4 cluster called the A-cluster.^{11–13} The oxidized A_{ox} state (corresponding to $[\text{Fe}_4\text{S}_4]^{2+}\text{-X-Ni}^{2+}$) can be reduced by

* To whom correspondence should be addressed. E-mail: Lindahl@mail.chem.tamu.edu.

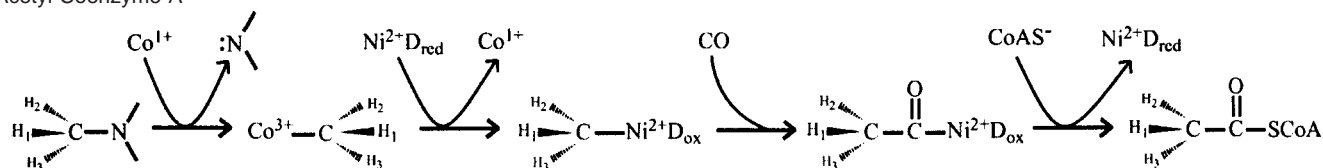
[‡] Department of Chemistry.

[†] Department of Biochemistry and Biophysics.

- (1) Wilson, G. G.; Murray, N. E. *Annu. Rev. Genet.* **1991**, *25*, 585–627.
- (2) Cheng, X. *Annu. Rev. Biophys. Biomol. Struct.* **1995**, *24*, 293–318.
- (3) Ludwig, M. L.; Matthews, R. G. *Annu. Rev. Biochem.* **1997**, *66*, 269–313.
- (4) Lindahl, P. A.; Chang, B. *Origins Life Evol. B* **2001**, *31*, 403–434.
- (5) Ferry, J. G. *Fems Microbiol. Rev.* **1999**, *23*, 13–38.
- (6) Ragsdale, S. W.; Kumar, M. *Chem. Rev.* **1996**, *96*, 2515–2539.
- (7) Abbreviations: ACS, acetyl-coenzyme A synthase, also known as CODH, carbon monoxide dehydrogenase; ACS_{red} and ACS_{ox} , ACS with the D-site reduced and oxidized, respectively; Phen-ACS, ACS treated with 1,10-phenanthroline; CoFeSP, Corrinoid-Iron-Sulfur Protein; MeTr, methyl-transferase; DTT, dithiothreitol; SDS-PAGE, sodium dodecyl sulfate polyacrylamide gel electrophoresis; CoA, coenzyme A.; ODE, ordinary differential equation; ASA, adapted simulated annealing.

- (8) Barondeau, D. P.; Lindahl, P. A. *J. Am. Chem. Soc.* **1997**, *119*, 3959–3970.
- (9) Pezacka, E.; Wood, H. G. *J. Biol. Chem.* **1988**, *263*, 16000–16003.
- (10) Lu, W.-P.; Harder, S. R.; Ragsdale, S. W. *J. Biol. Chem.* **1990**, *265*, 3124–3133.
- (11) Xia, J.; Lindahl, P. A. *J. Am. Chem. Soc.* **1996**, *118*, 483–484.
- (12) Xia, J.; Hu, Z.; Popescu, C. V.; Lindahl, P. A.; Münck, E. *J. Am. Chem. Soc.* **1997**, *119*, 8301–8312.
- (13) Russell, W. K.; Stålhandske, C. M. V.; Xia, J. Q.; Scott, R. A.; Lindahl, P. A. *J. Am. Chem. Soc.* **1998**, *120*, 7502–7510.

Scheme 1. Apparent Stereochemical Configuration of Methyl Group during Transfer from Methyltetrahydrofolate (on left) to Acetyl-Coenzyme A



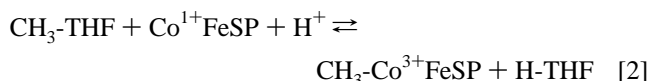
$1e^-$ and bound with CO to form the $S = 1/2$ $A_{red}\text{-CO}$ state ($[\text{Fe}_4\text{S}_4]^{2+}\text{-X-Ni}^{1+}\text{-CO}$).^{12,13} Contradictory roles for $A_{red}\text{-CO}$ have been proposed, including as an intermediate of catalysis^{14,15} and an inhibited state.^{8,16} We favor the latter, as the $A_{red}\text{-CO}$ state cannot be methylated.⁸ Moreover, CO at concentrations sufficient to elicit this state inhibits catalysis.¹⁷

The reduction event required for methylation was initially thought to correspond to the reaction $A_{ox} \rightarrow A_{red}\text{-CO}$. However, Barondeau and Lindahl found that reductants *unable* to generate $A_{red}\text{-CO}$ from A_{ox} *could* nevertheless cause methylation.⁸ They also found that the electronic spin state of $\text{CH}_3\text{-ACS}_{ox}$ ($S = 0$ or integer) was inconsistent with that expected if $A_{red}\text{-CO}$ had been methylated, and concluded that reduction involved 2 electrons. They proposed that a low-potential redox-active cystine/cysteine pair called the D-site must be reduced for methylation to occur. However, there is no direct spectroscopic evidence for this site.

Evidence that the methyl group is transferred to the Ni ion of the A-cluster is substantial though also indirect. This Ni ion is labile, and can be selectively removed by treatment with 1, 10-phenanthroline (phen).¹⁸ The resulting phen-ACS is catalytically inactive and probably unable to bind CO at the Ni-free A-cluster. Activity returns after phen-ACS is incubated in aqueous Ni^{2+} ions, as Ni^{2+} can reinsert into the vacant site of the A-cluster. Last, phen-ACS cannot be methylated, and methylation inhibits removal of Ni^{2+} by phen.⁸ If a stable $\text{CH}_3\text{-Ni}$ bond indeed forms, it, along with what appears to be a $\text{CH}_3\text{-Ni}$ bond in an intermediate state of methyl-coenzyme M reductase,¹⁹ would constitute only the second class of organometallic (M-alkyl) bonds found in living systems (the first involving cobalamins).

Kumar et al. have shown that $\text{Co}^{1+}\text{FeSP}$ is produced after the methyl group transfers from $\text{CH}_3\text{-Co}^{3+}\text{FeSP}$ to ACS_{red} .²⁰ The concentration of $\text{CH}_3\text{-Co}^{3+}\text{FeSP}$ declines at the same rate as $[\text{Co}^{1+}\text{FeSP}]$ increases, suggesting an $\text{S}_{\text{N}}2$ -based nucleophilic displacement in which a methyl cation is transferred in a single step, reaction 1. ACS_{red} and $\text{CH}_3\text{-ACS}_{ox}$ likely correspond to $\{\text{Ni}^{2+}\text{D}_{red}\}$ and $\{\text{CH}_3\text{-Ni}^{2+}\text{D}_{ox}\}$, respectively. A radical mechanism has also been suggested for the methyl group transfer.^{21,22} However, the stereochemical configuration of the methyl group is retained as it transfers from $\text{CH}_3\text{-THF}$ to $\text{CH}_3\text{-C(O)CoA}$, implying an even number of $\text{S}_{\text{N}}2$ methyl group transfers in the

overall reaction.²³ The first transfer, reaction 2, probably



involves an $\text{S}_{\text{N}}2$ nucleophilic displacement of the methyl group by the Co^{1+} ion. This would invert the methyl group stereochemistry.²⁴ The transfer described by [1] would also invert the methyl group configuration while subsequent steps, including CO insertion into the $\text{CH}_3\text{-Ni}^{2+}$ bond and attack of the resulting Ni-bound acetyl group by the thiolate of CoA, would not. Thus, methyl group stereochemistry in $\text{CH}_3\text{-THF}$ would be retained in the product, as illustrated in Scheme 1. Mechanisms involving another inversion step would afford inverted configurations, while radical-based mechanisms would yield racemic mixtures.

Ni complexes with properties relevant to this chemistry have been synthesized. $[\text{Ni}^{2+}(\text{N}(\text{CH}_2\text{CH}_2\text{SCH}(\text{CH}_3)_2)_3)(\text{Cl})]^{1+}$ reacts with CH_3MgCl to yield a $\text{CH}_3\text{-Ni}^{2+}$ adduct into which CO inserts.²⁵ The resulting $\text{CH}_3\text{C(O)-Ni}^{2+}$ complex reacts with thiolates, yielding thioesters of acetic acid and Ni^0 . Although the reaction sequence is similar to that proposed for ACS, a methyl anion (rather than a cation) transfers onto Ni^{2+} , ultimately yielding Ni^0 (rather than Ni^{2+}) when product forms. Another relevant example involves $\text{CH}_3\text{-Co}^{3+}(\text{difluoroboryl})\text{-dimethylglyoximate}_2\text{py}$. The methyl group of this complex transfers to $[\text{Ni}^{1+}(1,4,8,11\text{-tetraazacyclotetradecane})]^{1+}$, albeit by a radical-based mechanism.^{21,22}

Our interest in the catalytic mechanism of ACS and the novelty of its methyl group transfer reaction prompted us to examine the kinetics of reaction 1. Although a preliminary study of the kinetics of [1] had been reported,²⁰ a more detailed exploration was anticipated to afford further mechanistic insight. In this paper, we report that the reaction occurs reversibly and is inhibited by CO. Forward and reverse rate constants were determined, allowing the equilibrium constant to be calculated.

Experimental Procedures

Preparation of Proteins. *C. thermoaceticum* cells were grown in a 25 L bioreactor, harvested anaerobically, and stored at -80°C as described.^{8,26} ACS, CoFeSP, and MeTr (154 700 g/mol $\alpha\beta$, 89 000 g/mol $\alpha\beta$, and 57 280 g/mol α_2 , respectively) were purified from cell paste^{8,17} using an Ar-atmosphere glovebox (Vac/Atm HE-453) with <1 ppm O_2 , monitored continuously with a calibrated analyzer (Teledyne model 310A). Dithionite-reduced proteins were frozen in liquid N_2 . Portions were thawed, subjected to Sephadex G25 chromatography (1 cm \times 20 cm; equilibrated in Buffer A (50 mM Tris pH 8.0 and 1 mM DTT) at 0.5 mL/min), divided into aliquots, and refrozen in liquid N_2 .

- (23) Lebertz, H.; Simon, H.; Courtney, L. F.; Benkovic, S. J.; Zydowsky, L. D.; Lee, K.; Floss, H. G. *J. Am. Chem. Soc.* **1987**, *109*, 3173–3174.
 (24) Seravalli, J.; Zhao, S. Y.; Ragsdale, S. W. *Biochemistry* **1999**, *38*, 5728–5735.
 (25) Tucci, G. C.; Holm, R. H. *J. Am. Chem. Soc.* **1995**, *117*, 6489–6496.
 (26) Lundie, L. L., Jr.; Drake, H. L. *J. Bacteriol.* **1984**, *159*, 700–703.

(14) Gorst, C. M.; Ragsdale, S. W. *J. Biol. Chem.* **1991**, *266*, 20687–20693.

(15) Menon, S.; Ragsdale, S. W. *J. Biol. Chem.* **1999**, *274*, 11513–11518.

(16) Grahame, D. A.; Khangulov, S.; DeMoll, E. *Biochemistry* **1996**, *35*, 593–600.

(17) Maynard, E. L.; Sewell, C.; Lindahl, P. A. *J. Am. Chem. Soc.* **2001**, *123*, 4697–4703.

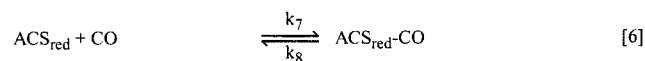
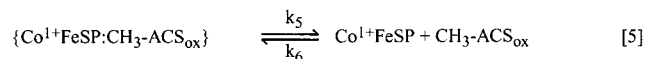
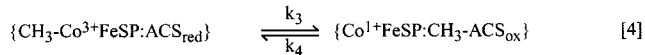
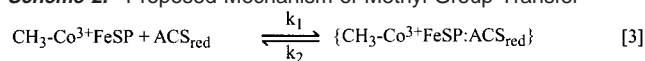
(18) Shin, W.; Lindahl, P. A. *J. Am. Chem. Soc.* **1992**, *114*, 9718–9719.

(19) Ermler, U.; Grabarse, W.; Shima, S.; Goubeaud, M.; Thauer, R. K. *Science* **1997**, *278*, 1457–1462.

(20) Kumar, M.; Qiu, D.; Spiro, T. G.; Ragsdale, S. W. *Science* **1995**, *270*, 628–630.

(21) Ram, M. S.; Riordan, C. G. *J. Am. Chem. Soc.* **1995**, *117*, 2365–2366.

(22) Ram, M. S.; Riordan, C. G.; Yap, G. P. A.; Liable-Sands, L.; Rheingold, A. L.; Marchaj, A.; Norton, J. R. *J. Am. Chem. Soc.* **1997**, *119*, 1648–1655.

Scheme 2. Proposed Mechanism of Methyl Group Transfer

until needed. Protein concentrations were determined as described.²⁷ Each protein was >95% pure, as quantified by imaging Coomassie-Blue (Bio-Rad)-stained SDS-PAGE gels (Alpha Innotech Imager 2000). ACS catalyzed CO oxidation²⁸ and acetyl-CoA synthesis¹⁷ with specific activities of 320 $\mu\text{mol min}^{-1} \text{mg}^{-1}$ and 1.2 $\mu\text{mol min}^{-1} \text{mg}^{-1}$, respectively.

Methylation of CoFeSP and ACS. Ti^{3+} citrate was prepared from TiCl_3 (Aldrich)²⁹ and standardized by titration against $\text{K}_3[\text{Fe}(\text{CN})_6]$. $\text{Co}^{1+}\text{FeSP}$ was methylated using $\text{CH}_3\text{-THF}$ (Sigma) as described.⁸ Analysis indicated 0.95 $\text{Co}/\alpha\beta$ for a CoFeSP sample, and 0.99 $\text{Co}/\alpha\beta$ for a $\text{CH}_3\text{-Co}^{3+}\text{FeSP}$ sample.³⁰ ACS (200 $\mu\text{mol } \alpha\beta$) was methylated by adding a 20-fold molar excess of Ti^{3+} citrate, incubating 20 min, then adding $\text{CH}_3\text{-Co}^{3+}\text{FeSP}$ (230 $\mu\text{mol } \alpha\beta$). The reaction was monitored spectrophotometrically at 390 nm. After 1 h, $\text{CH}_3\text{-ACS}$ was separated from CoFeSP by phenyl sepharose chromatography. Resin (30 mL) was equilibrated with Buffer A containing 10% w/v $(\text{NH}_4)_2\text{SO}_4$. The reaction mixture in 10% $(\text{NH}_4)_2\text{SO}_4$ was loaded on the column (2 cm \times 20 cm) and washed with Buffer A containing 10% $(\text{NH}_4)_2\text{SO}_4$. CoFeSP was eluted with Buffer A containing 2.5% $(\text{NH}_4)_2\text{SO}_4$, while $\text{CH}_3\text{-ACS}$ (and any unreacted ACS) was eluted with Buffer A. The resulting $\text{CH}_3\text{-ACS}_{\text{ox}}$ solution contained <5% CoFeSP, according to a densitometry analysis of an SDS-PAGE gel. $^{14}\text{CH}_3\text{-THF}$ and a scintillation counter (Beckman, LS 6000SE) were used in an equivalent experiment⁸ to determine that 0.5 CH_3 per ACS $\alpha\beta$ and 0.95 CH_3 per CoFeSP $\alpha\beta$ were methylated.

Stopped-Flow Experiments. Pre-steady-state experiments were performed at 25 °C with an SF-61 DX2 Double-Mixing Stopped-Flow instrument (Hi-Tech Limited, UK) installed in an Ar-atm glovebox (MJ Braun, Inc) with O_2 <1 ppm. Temperature was controlled by a circulating water bath (Neslab Instruments, RTE-110). Unless otherwise noted, reactions were monitored in PM mode at 390 nm. Freshly prepared sodium dithionite solutions were standardized vs $\text{K}_3[\text{Fe}(\text{CN})_6]$. Phen-ACS was prepared by incubating dithionite-free ACS (20 μM) in 200 μM phen for 1 h. Excess phen and presumably $\text{Ni}(\text{phen})_3$ were removed by Sephadex G25 chromatography. CO (MG Industries, research grade) and Ar were passed through Oxysorb (MG Industries) filters, mixed using a calibrated flowmeter (MG Industries, series 7941-AS2 4-tube), and passed into a reaction vessel¹⁷ containing protein solutions. Henry's law constant for CO at 30 °C is 0.98 mM/atm .³¹ Solutions were transferred to stopped-flow syringes by a custom-made cannula adapter.

Kinetic Simulations. A computer program was written to simulate the Abs_{390} -vs-time kinetic traces. Two mechanisms were considered, including reaction 1 and reactions 3–6, as shown in Scheme 2. Ordinary differential equations (ODE's) describing the time-dependent change of the concentration of each component were generated from these equations. Candidate rate constants and initial concentrations of proteins were generated by the Adapted Simulated Annealing (ASA) method,

limited within specified min/max values.³² For a given set of rate constants and initial concentrations, ODE's were solved numerically using a fourth-order Runge–Kutta.³³ Using ASA, candidate electronic absorption molar extinction coefficients at 390 nm for each protein component were similarly generated, and these were used to convert simulated concentration-vs-time plots into corresponding absorbance-vs-time plots. Plots were quantitatively compared to experimental traces by calculating the sum of the squares of the residuals defined by [7].

$$Q = \sum (\text{Abs}_{390\text{-dat}} - \text{Abs}_{390\text{-sim}})^2 \quad [7]$$

Additional ASA-generated rate constants, initial protein concentrations, and extinction coefficients were generated, and the process was iterated until Q was minimized. Resulting values were deemed “best-fit”.

Candidate protein concentrations were within $\pm 0.5 \mu\text{M}$ of their experimentally determined values. Candidate extinction coefficients were $\pm \sim 20\%$ of their experimentally determined values (except for two coefficients which could not be determined experimentally—see Table 1). With improvements in fits, these limits were eventually set to $\pm < 10\%$. Allowing these parameters to vary within the uncertainty of their experimentally determined values improved fits. For rate constants, min/max limits were initially set liberally (from 10^{-4} – 10^2), but were gradually restricted as fits improved. The Hi-Tech software fitting package (KinetAsyst 2) was also used to fit experimental traces when first-order processes were assumed.

The [CoFeSP] used in simulations as center experimental values were $1/2$ of those measured (before mixing). The “[ACS]” values used were $1/4$ of those measured, so as to represent the concentration of functional Ni ions in the samples. ACS is heterogeneous such that only $\sim 1/2$ of the $\alpha\beta$ dimeric units are catalytically functional.³⁴

Experiments were performed using two independent batches of ACS, CoFeSP, and MT proteins, called B1 and B2. For each batch, best-fit rate constants for data sets were averaged, standard deviations were determined, and a sensitivity analysis was performed (Table 2). The sensitivity analysis involved varying each free-floating parameter, one at a time around its best-fit value, while fixing all other parameters at their best-fit values. Values that yielded $Q = 1.5Q_{\text{best-fit}}$, called k_+ and k_- , were determined and their averaged values are given in Table 2. “Overall Estimates” consisted of the averaged best-fit k -value for both batches and an uncertainty estimate defined as $\{\text{SD} + \text{SP}\}/2$, where SD is the standard deviation of each k -value and SP is defined as $\{(k_+ - k_-)_{\text{B1}} + (k_+ - k_-)_{\text{B2}}\}/4$.

Results

The objectives of this study were to (a) examine the kinetics by which the methyl group of $\text{CH}_3\text{-Co}^{3+}\text{FeSP}$ transfers to reduced ACS, (b) formulate the reaction mechanism for that process, and (c) obtain microscopic rate constants associated with each mechanistic step. Under the conditions employed, the greatest absorbance difference occurred at 390 nm (Figure 1), and so extinction coefficients of the products and reactants (ϵ_{390}) were determined at this wavelength (Table 1). $\text{Co}^{1+}\text{FeSP}$ and $\text{CH}_3\text{-Co}^{3+}\text{FeSP}$ exhibited the greatest difference in ϵ_{390} values and were largely responsible for the absorbance changes observed during the reaction.

In the first set of experiments, Ti^{3+} citrate-reduced ACS (ACS_{red}) and $\text{CH}_3\text{-Co}^{3+}\text{FeSP}$ were mixed and monitored at A_{390} (Figure 2A). Significant absorption differences were also observed at 450 nm, so equivalent stopped-flow traces were obtained at this wavelength (Figure 2B). Under these conditions,

(27) Pelley, J. W.; Garner, C. W.; Little, G. H. *Anal. Biochem.* **1978**, *86*, 341–343.

(28) Shin, W.; Lindahl, P. A. *Biochem. Biophys.* **1993**, *1161*, 317–322.

(29) Seefeldt, L. C.; Ensign, S. A. *Anal. Biochem.* **1994**, *221*, 379–386.

(30) Ljungdahl, L. G.; LeGall, J.; Lee, J.-P. *Biochemistry* **1973**, *12*, 1802–1806.

(31) Budavari, S. *The Merck Index*, 11th ed.; Merck & Co. Inc.: Rahway, NJ, 1989.

(32) Ingber, L. *Control Cybernet.* **1996**, *25*, 33–54.

(33) Shoup, T. E. *Applied Numerical Methods for the Microcomputer*; Prentice-Hall: Englewood Cliffs, NJ, 1984.

(34) Fraser, D. M.; Lindahl, P. A. *Biochemistry* **1999**, *38*, 15697–15705.

Table 1. Extinction Coefficients at 390 and 450 nm (in $\mu\text{M}^{-1} \text{cm}^{-1}$)

| reactant | measured | | best-fit | |
|---|----------|--------|-----------------|-----------------|
| | 390 nm | 450 nm | 390 nm | 450 nm |
| CH ₃ -Co ³⁺ FeSP | 0.0105 | 0.0047 | 0.0102 ± 0.0005 | 0.0050 ± 0.0005 |
| Co ¹⁺ FeSP | 0.0192 | 0.0037 | 0.0193 ± 0.0005 | 0.0035 ± 0.0005 |
| ACS _{red} (with Ti ³⁺ citrate) | 0.0212 | 0.0196 | 0.0205 ± 0.0005 | 0.0196 ± 0.0005 |
| CH ₃ -ACS _{ox} | 0.0219 | 0.0187 | 0.0215 ± 0.0005 | 0.0190 ± 0.0005 |
| CH ₃ -Co ³⁺ FeSP:ACS _{red} | | | 0.0360 ± 0.0005 | 0.0220 ± 0.0005 |
| Co ¹⁺ FeSP:CH ₃ -ACS _{ox} | | | 0.0375 ± 0.0005 | 0.0215 ± 0.0005 |
| ACS _{red} -CO | 0.0190 | | 0.0185 ± 0.0005 | |
| Ti ³⁺ citrate | 0.00013 | | | |
| Ti ⁴⁺ citrate | 0.00078 | | | |

Table 2. Best-Fit Parameters and Sensitivity Analysis

| no. | [CO] ^e | [CH ₃ CP] ^e | | [labile Ni] ^e | | [Ti ³⁺] ^e | k ₁ ^f | k ₂ ^g | k ₃ ^g | k ₄ ^g | k ₅ ^g | k ₆ ^f | k ₇ ^f | k ₈ ^g |
|--------------------|-------------------|-----------------------------------|----------|--------------------------|----------|----------------------------------|-----------------------------|-----------------------------|-----------------------------|-----------------------------|-----------------------------|-----------------------------|-----------------------------|-----------------------------|
| | | exp | best fit | exp | best fit | | | | | | | | | |
| 1 | | 3.0 | 3.2 | 3.8 | 3.8 | 100 | 9.7 | 1.0 | 6.6 | 2.7 | 0.1 | 0.6 | | |
| 2 | | 3.0 | 3.3 | 3.8 | 3.6 | 1000 | 10.4 | 1.0 | 6.5 | 2.8 | 0.1 | 0.6 | | |
| 3 | | 3.0 | 3.3 | 3.8 | 4.0 | 200 ^d | 9.5 | 1.0 | 6.5 | 2.8 | 0.3 | 0.6 | | |
| 4 | 0 | 2.5 | 2.6 | 3.8 | 3.7 | 200 | 10.5 | 1.0 | 6.5 | 2.8 | 0.1 | 0.6 | | |
| 5 | 40 | 2.5 | 2.7 | 3.8 | 3.8 | 200 | 10.5 | 1.2 | 6.5 | 2.6 | 0.1 | 0.5 | 0.2 | 34.8 |
| 6 | 100 | 2.5 | 2.8 | 3.8 | 3.8 | 200 | 10.5 | 1.0 | 6.5 | 2.6 | 0.1 | 0.6 | 0.1 | 35.9 |
| 7 | 0 | 2.5 | 2.3 | 3.8 | 3.3 | 200 | 9.6 | 0.8 | 6.0 | 2.8 | 0.1 | 0.8 | | |
| 8 | 120 | 2.5 | 2.8 | 3.8 | 3.9 | 200 | 9.3 | 1.3 | 6.7 | 3.2 | 0.1 | 0.6 | 0.2 | 37.8 |
| 9 | 200 | 2.5 | 2.6 | 3.8 | 3.6 | 200 | 9.8 | 1.0 | 6.4 | 3.0 | 0.1 | 0.6 | 0.1 | 37.8 |
| 10 | 490 | 2.5 | 2.4 | 3.8 | 3.8 | 200 | 10.0 | 1.4 | 6.8 | 2.5 | 0.1 | 0.6 | 0.1 | 37.9 |
| 11 | 490 ^d | 2.5 | 2.1 | 3.8 | 3.8 | 200 | 7.5 | 0.8 | 7.8 | 2.6 | 0.2 | 0.6 | 0.2 | 33.0 |
| 12 ^b | | 5.0 | 5.3 | 3.8 | 4.0 | - | 10.9 | 1.9 | 6.6 | 2.6 | 0.2 | 0.5 | | |
| 13 ^b | | 15.0 | 15.3 | 3.8 | 3.8 | 200 | 9.5 | 2.8 | 6.6 | 2.6 | 0.3 | 0.5 | | |
| 14 | | 5.0 | 5.1 | 5.0 | 5.4 | 200 | 7.5 | 0.8 | 7.9 | 3.4 | 0.1 | 0.7 | | |
| 15 | | 5.0 | 5.4 | 5.0 | 5.4 | 400 | 7.5 | 0.8 | 7.9 | 2.9 | 0.1 | 0.7 | | |
| 16 | | 5.0 | 5.0 | 5.0 | 5.0 | 1000 | 8.2 | 1.3 | 6.6 | 3.4 | 0.1 | 0.7 | | |
| 17 ^c | | 5.0 | 4.7 | 5.0 | 5.4 | 1000 | 8.0 | 1.4 | 6.7 | 3.1 | 0.2 | 0.5 | | |
| 18 | | 5.0 | 5.2 | 5.0 | 4.8 | 5000 | 7.9 | 0.8 | 6.5 | 3.3 | 0.1 | 0.8 | | |
| 19 | | 2.5 | 2.3 | 10.0 | 9.9 | 1000 | 9.2 | 0.5 | 6.9 | 3.7 | 0.1 | 0.5 | | |
| 20 | | 5.0 | 5.2 | 10.0 | 10.1 | 1000 | 7.5 | 0.9 | 8.0 | 3.4 | 0.1 | 0.8 | | |
| 21 | | 10.0 | 9.8 | 10.0 | 10.3 | 1000 | 7.5 | 1.0 | 8.0 | 3.5 | 0.1 | 0.7 | | |
| 22 | | 5.0 | 4.7 | 2.5 | 2.9 | 1000 | 7.0 | 0.8 | 7.9 | 2.1 | 0.1 | 0.7 | | |
| 23 | | 5.0 | 5.4 | 7.5 | 7.8 | 1000 | 7.1 | 0.8 | 7.1 | 3.0 | 0.1 | 0.6 | | |
| 24 | | 7.5 | 7.4 | 7.5 | 7.7 | 1000 | 7.0 | 1.0 | 6.1 | 3.8 | 0.1 | 0.6 | | |
| av k | | | | | | | 8.9 | 1.1 | 6.9 | 3.0 | 0.1 | 0.6 | 0.2 | 36.2 |
| SD (±) | | | | | | | 1.3 | 0.5 | 0.6 | 0.4 | 0.1 | 0.1 | 0.1 | 1.3 |
| B1, k ₋ | | | | | | | 9.4 | 1.2 | 4.6 | 1.7 | 0.1 | 0.3 | 0.2 | 31.7 |
| B1, k ₊ | | | | | | | 12 | 2.0 | 9.8 | 4.3 | 0.4 | 0.6 | 0.3 | 39.6 |
| B2, k ₋ | | | | | | | 6.4 | 0.6 | 5.1 | 2.5 | 0.1 | 0.3 | 0.1 | 32.0 |
| B2, k ₊ | | | | | | | 10.2 | 1.5 | 10.3 | 6.3 | 0.3 | 0.9 | 0.4 | 40.0 |
| overall estimate | | | | | | | 8.9 ± 1.5 | 1.1 ± 0.5 | 6.9 ± 1.6 | 3.0 ± 1.0 | 0.2 ± 0.1 | 0.6 ± 0.2 | 0.2 ± 0.1 | 36.2 ± 2.0 |

^a [CH₃Co³⁺FeSP] and [ACS] were reduced by dithionite rather than by Ti³⁺citrate. ^b The reverse reaction was probed and protein concentrations refer to [Co¹⁺FeSP] and [CH₃ACS_{ox}]. ^c Monitored at 450 nm, while all other experiments were monitored at 390 nm. ^d CO was in the ACS syringe, while in other cases CO was in the CH₃Co³⁺FeSP syringe. Experiments 1–6, 11, and 12 used the first batch of proteins (B1), while experiments 7–11 and 14–24 used the second batch (B2). [CO], [CH₃Co³⁺FeSP]/[Co¹⁺FeSP], [labile Ni]/[CH₃ACS_{ox}], and [Ti³⁺citrate] are final concentrations after mixing. k₁–k₁₀ are microscopic rate constants for the reactions 3–6. ^e Units: μM . ^f Units: $\mu\text{M}^{-1} \text{s}^{-1}$. ^g Units: s^{-1} .

the reaction essentially reached equilibrium within ~ 1 s. Simulations of the two traces using the three-step model described below (and in Scheme 2) yielded nearly identical best-fit rate constants (Table 2). This suggests that a single process was probed in these experiments, namely methyl group transfer. For maximal sensitivity and convenience, subsequent reactions were monitored at 390 nm.

Effects of reductants and protein concentration on reaction rates were examined. Rates depended on the concentrations of the proteins (Table 2) but were independent of the concentration of Ti³⁺citrate between 100 (Figure 3A) and 1000 μM (Figure 3B). The reaction occurred at a similar rate when sodium dithionite replaced Ti³⁺citrate as the reductant in the ACS-containing syringe (compare Figure 3, traces C and B). The methyl group transfer reaction did not occur in the absence of

either a reductant (Figure 3E) or the labile Ni of the A-cluster (Figure 3D). These results confirm previous studies indicating that a low-potential reductant and the Ni of the A-cluster are both required for methyl group transfer.⁸

To investigate the kinetics of the reverse reaction, CH₃-ACS_{ox} was incubated in Ti³⁺citrate and then mixed with Ti³⁺citrate-reduced Co¹⁺FeSP. However, no reaction was observed (Figure 4A). The methyl group of CH₃-ACS_{ox} did transfer to Co¹⁺-FeSP when reductant was absent (Figure 4B), reaching apparent equilibrium within ~ 2 s. A similar result obtained when reductant-free CH₃-ACS_{ox} was mixed with Ti³⁺citrate-reduced Co¹⁺FeSP (Figure 4C). Although the rate of the reactions differed (compare time scales of Figure 4, B and C), this was due to the different [Co¹⁺FeSP] used, not to the rate constant associated with the process (see Table 2). The important point

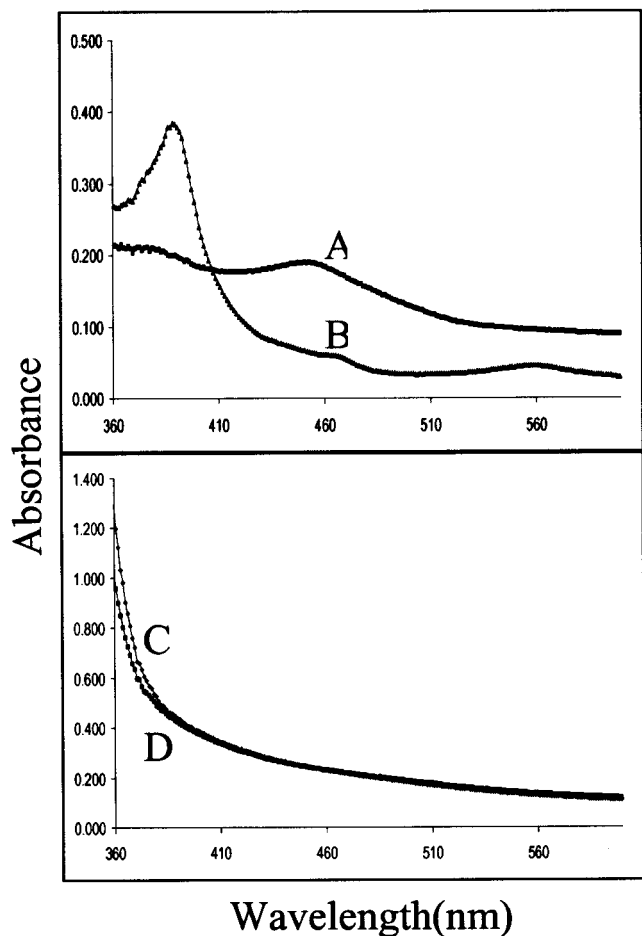


Figure 1. Electronic absorption spectra of (A) $\text{CH}_3\text{-Co}^{3+}\text{FeSP}$, (B) $\text{Co}^{1+}\text{FeSP}$, (C) $\text{CH}_3\text{-ACS}_{\text{ox}}$, and (D) ACS_{red} . Proteins ($20 \mu\text{M}$) were in 50 mM Tris-Cl, pH 8.0, plus $80 \mu\text{M}$ dithiothreitol (Buffer Z).

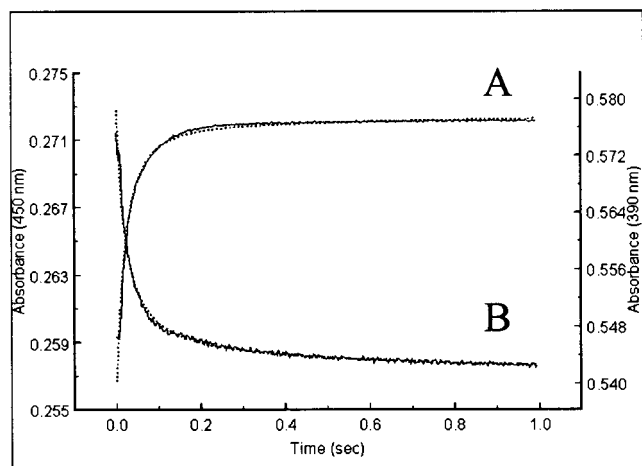


Figure 2. Reaction of ACS with $\text{CH}_3\text{-Co}^{3+}\text{FeSP}$, monitored at (A) 390 nm (right absorbance axis) and (B) 450 nm (left absorbance axis). ACS ($20 \mu\text{M}$) in Buffer Z was preincubated with Ti^{3+} -citrate ($1000 \mu\text{M}$) for 20 min and mixed with $\text{CH}_3\text{-Co}^{3+}\text{FeSP}$ ($10 \mu\text{M}$) that had been similarly preincubated. Dashed lines: Best-fit simulations using reactions 3–5 and parameters in Tables 1 and 2. Simulations for A and B correspond to Nos. 16 and 17 of Table 2, respectively.

is that Ti^{3+} citrate inhibited the reaction when it was preincubated with $\text{CH}_3\text{-ACS}_{\text{ox}}$ but not when it was preincubated with $\text{Co}^{1+}\text{-FeSP}$. Ti^{3+} citrate probably reduces $\text{CH}_3\text{-ACS}_{\text{ox}}$, affording a state that cannot donate the methyl group to $\text{Co}^{1+}\text{FeSP}$.

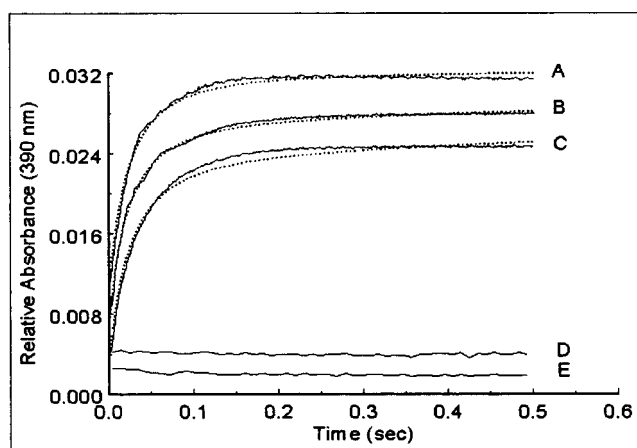


Figure 3. Effect of reductant and labile Ni on rates of methyl group transfer. Solid lines: (A) ACS ($15 \mu\text{M}$) and Ti^{3+} citrate ($100 \mu\text{M}$) in Buffer Z incubated for 20 min before mixing with $\text{CH}_3\text{-Co}^{3+}\text{FeSP}$ ($6.0 \mu\text{M}$) and Ti^{3+} citrate ($100 \mu\text{M}$) in Buffer Z; (B) same as A except that $[\text{Ti}^{3+}\text{citrate}] = 1000 \mu\text{M}$; (C) same as A except that dithionite ($200 \mu\text{M}$) replaced Ti^{3+} citrate; (D) same as A except that Phen-ACS ($20 \mu\text{M}$) replaced ACS and $[\text{Ti}^{3+}\text{citrate}] = 500 \mu\text{M}$; (E) same as A except that Ti^{3+} citrate was absent. Dash lines: Best-fit simulations using reactions 3–5 and parameters given in Tables 1 and 2. Simulations for A, B, and C correspond to Nos. 1, 2, and 3 of Table 2, respectively.

A similar result was obtained when sodium dithionite rather than Ti^{3+} citrate was used as the low-potential reductant in the reverse reaction. When dithionite was preincubated with $\text{CH}_3\text{-ACS}_{\text{ox}}$, no reaction occurred (data not shown but trace was like Figure 4A). Thus, dithionite also inhibited methyl group transfer, apparently by reducing $\text{CH}_3\text{-ACS}_{\text{ox}}$. When dithionite was preincubated with $\text{Co}^{1+}\text{FeSP}$ and then mixed with reductant-free $\text{CH}_3\text{-ACS}_{\text{ox}}$, the absorbance increased in the first few seconds and then decreased in $\sim 200 \text{ s}$ as the methyl group very slowly transferred and the system approached equilibrium (Figure 4D). We do not understand why the absorbance initially increased, but the slow subsequent decline seems analogous to that observed with Ti^{3+} citrate, and almost certainly corresponds to methyl group transfer. Inhibition by dithionite may be more “potent” than that with Ti^{3+} citrate, as the methyl group transfer rate was ~ 200 -fold slower (compare time scales of Figure 4, C and D).

The effect of the substrate and reductant CO was evaluated in the final set of experiments. When different concentrations of CO were included in the syringe containing $\text{CH}_3\text{-Co}^{3+}\text{FeSP}$, rates of methyl group transfer to ACS_{red} declined as CO concentrations increased (Figure 5, A–F). These results indicate that CO inhibits the reaction. The slowest rate of methyl group transfer was obtained when CO was included in the ACS_{red} syringe (Figure 5G). The difference in rate between F and G (both of which have the same final concentration of CO, namely $490 \mu\text{M}$) suggests that the rate at which CO binds ACS_{red} is slow relative to that at which the methyl group transfers from $\text{CH}_3\text{-Co}^{3+}\text{FeSP}$ to ACS_{red} . This is congruent with the slow rate at which the $S = 1/2$ $\text{A}_{\text{red}}\text{-CO}$ state of the A-cluster develops upon exposing ACS to CO.^{35, 36}

We attempted to simulate the forward and reverse methyl group transfer data assuming reaction 1. Accordingly, time-

(35) Anderson, M. E.; Lindahl, P. A. *Biochemistry* **1994**, *33*, 8702–8711.

(36) Kumar, M.; Lu, W.-P.; Ragsdale, S. W. *J. Am. Chem. Soc.* **1993**, *115*, 11646–11647.

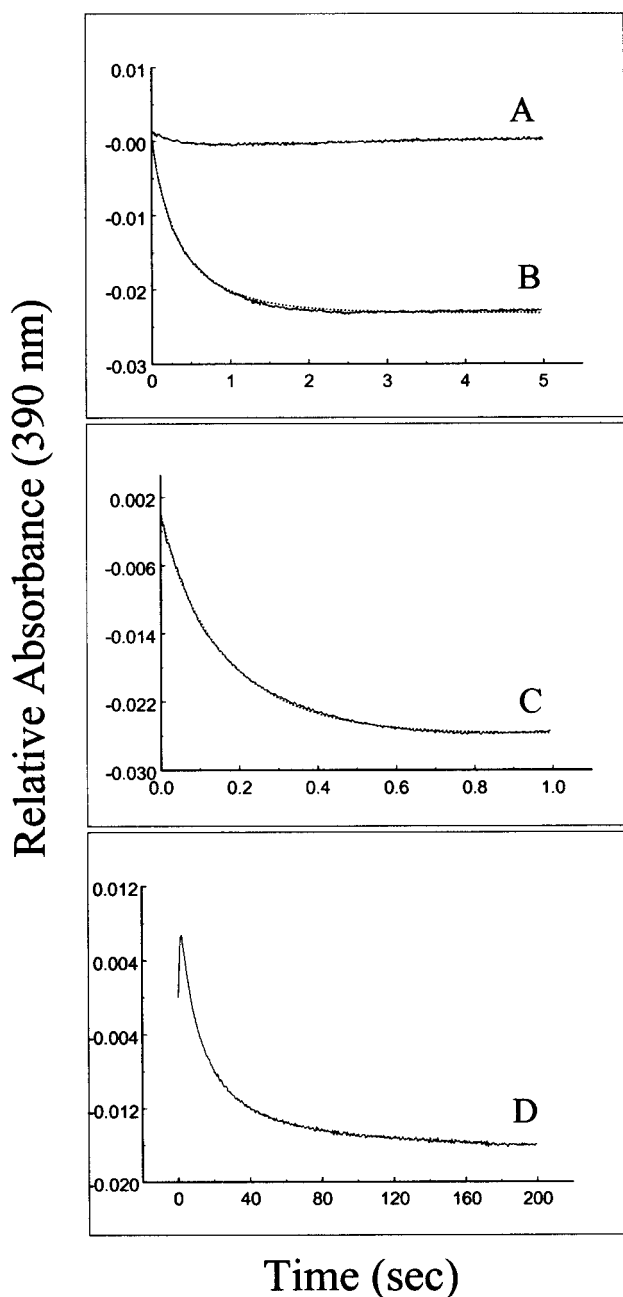


Figure 4. Kinetics of the reverse methyl group transfer reaction. Solid lines: (A) $\text{CH}_3\text{-ACS}_{\text{ox}}$ ($15 \mu\text{M}$) and Ti^{3+} citrate ($500 \mu\text{M}$) in buffer Z were incubated for 20 min, then mixed with $\text{Co}^{1+}\text{FeSP}$ ($10 \mu\text{M}$) and Ti^{3+} citrate ($500 \mu\text{M}$) in Buffer Z; (B) same as A except that Ti^{3+} citrate was absent; (C) same as B except that Ti^{3+} citrate ($400 \mu\text{M}$) was included with the $\text{Co}^{1+}\text{FeSP}$ ($30 \mu\text{M}$) for 20 min before mixing; (D) same as C except that dithionite ($400 \mu\text{M}$) replaced the Ti^{3+} citrate. Dash lines: Best-fit simulations using reactions 3–5 and parameters given in Tables 1 and 2. Simulations for B and C correspond to Nos. 12 and 13, respectively.

dependent concentration changes were given in [8]. Equation 8

$$\frac{d[\text{CH}_3\text{ACS}_{\text{ox}}]}{dt} = \frac{d[\text{Co}^{1+}\text{FeSP}]}{dt} = -\frac{d[\text{CH}_3\text{Co}^{3+}\text{FeSP}]}{dt} = -\frac{d[\text{ACS}_{\text{red}}]}{dt} = k_f[\text{CH}_3\text{Co}^{3+}\text{FeSP}][\text{ACS}_{\text{red}}] - k_r[\text{CH}_3\text{ACS}_{\text{ox}}][\text{Co}^{1+}\text{FeSP}] \quad [8]$$

was numerically integrated and the resulting simulation was

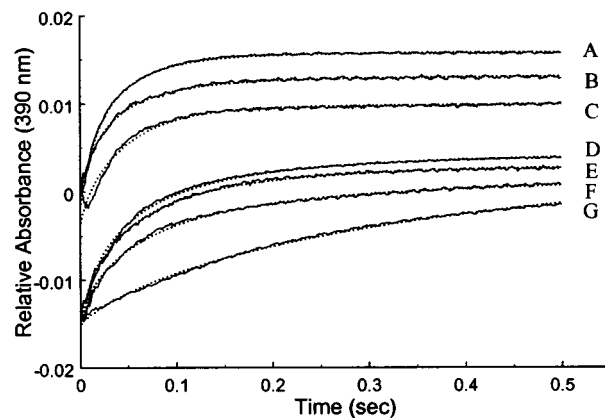


Figure 5. Effect of CO on methyl group transfer. Solid lines: ACS ($15 \mu\text{M}$) and Ti^{3+} citrate ($200 \mu\text{M}$) in buffer Z were incubated for 15 min. $\text{CH}_3\text{-Co}^{3+}\text{FeSP}$ ($5.0 \mu\text{M}$) and Ti^{3+} citrate ($200 \mu\text{M}$) in Buffer Z were incubated under (A) 0, (B) 80, (C) 200, (D) 240, (E) 400, and (F) $980 \mu\text{M}$ [CO] for 15 min, and the two solutions were mixed. (G) ACS ($15 \mu\text{M}$) in buffer Z containing $200 \mu\text{M}$ Ti^{3+} citrate was incubated with $980 \mu\text{M}$ [CO] for 15 min, and then mixed with $\text{CH}_3\text{Co}^{3+}\text{FeSP}$ ($5.0 \mu\text{M}$) and Ti^{3+} citrate ($200 \mu\text{M}$) in Buffer Z. Dash lines: Best-fit simulations using reactions 3–6 and parameters listed in Tables 1 and 2. Simulations for A, B, C, D, E, F, and G correspond to Nos. 4, 5, 6, 8, 9, 10, and 11 of Table 2, respectively. A, B, and C were obtained using the first batch of protein, while D, E, F, and G were obtained using the second batch of protein.

fitted to the data as described in Experimental Procedures. Fits to the forward-reaction traces (Figure 3, A–C) yielded best-fit values $k_f \sim 7 \mu\text{M}^{-1} \text{s}^{-1}$ and $k_r \sim 1.6 \mu\text{M}^{-1} \text{s}^{-1}$. However, fits to the reverse-reaction traces (Figure 4, B and C) yielded substantially different best-fit values, namely $k_f \sim 0.1 \mu\text{M}^{-1} \text{s}^{-1}$ and $k_r \sim 0.5 \mu\text{M}^{-1} \text{s}^{-1}$.

A consistent set of best-fit parameters was obtained by employing a three-step mechanism (reactions 3–5) that involved (a) binding of $\text{CH}_3\text{-Co}^{3+}\text{FeSP}$ and ACS_{red} to form a “pre-transfer” complex, (b) intracomplex methyl group transfer, and (c) dissociation of a “post-transfer” complex into $\text{Co}^{1+}\text{FeSP}$ and $\text{CH}_3\text{-ACS}_{\text{ox}}$. This mechanism fit all experimental traces well, yielding the dotted lines overlaying the data in these figures and the best-fit values given in Table 2.

The CO-dependent data of Figure 5 (A–G) were simulated using the same model but augmented by reaction 6, a CO-binding step. Resulting best-fit simulations are the dotted lines in Figure 5, using parameters listed in Tables 1 and 2. Additional CO-binding steps did not improve fits. In simulating the trace in Figure 5G (in which CO was preincubated in the ACS syringe), the enzyme was assumed to be entirely in the ACS_{red} -CO form at the time of mixing with $\text{CH}_3\text{-Co}^{3+}\text{FeSP}$.

Discussion

In this study we have characterized the kinetics of methyl group transfer between the cobalt of the CoFeSP and the Ni of the A-cluster of ACS. This is an exceptional reaction in biology, in that both methyl group donor and acceptor appear to be metal ions. We found that the reaction is reversible, with the rate constant in the forward direction ($k_f = 6.9 \text{s}^{-1}$ for $\{\text{CH}_3\text{-Co}^{3+}:\text{Ni}^{2+}\text{D}_{\text{red}}\} \rightarrow \{\text{Co}^{1+}:\text{CH}_3\text{-Ni}^{2+}\text{D}_{\text{ox}}\}$) being more than twice as fast as that in the reverse reaction ($k_r = 3.0 \text{s}^{-1}$). The ratio of these two values yields the thermodynamic equilibrium constant, $K_{\text{eq}} = 2.3 \pm 0.9$. Our simulations suggest that the reaction is first order in ACS and CoFeSP, and that the transfer occurs within a complex formed between the two proteins. CO inhibits

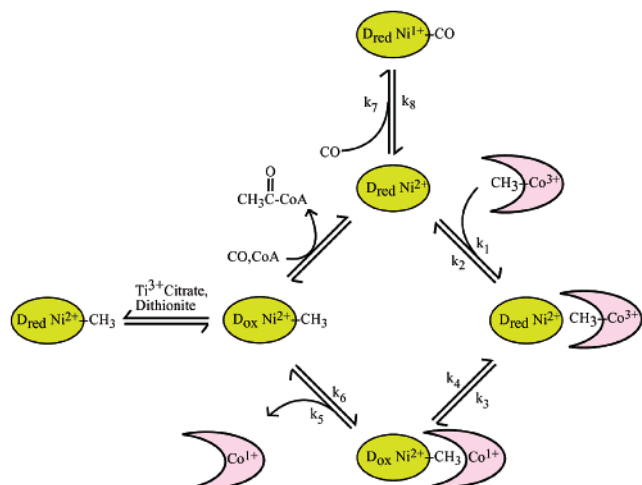


Figure 6. Proposed mechanism of acetyl-CoA synthesis by ACS, emphasizing the methyl group transfer reaction with CoFeSP and inhibition by CO and reductants. The central “diamond” region represents the catalytic cycle, while the two reactions emanating from this region indicate inhibition steps. Best-fit rate constants for all steps are given in Table 2. ACS with the A-cluster oxidized and the D-site reduced (central mid-level green ellipse labeled $D_{\text{red}}\text{Ni}^{2+}$) can bind CO, yielding the $A_{\text{red}}\text{-CO}$ state, designated by $\text{Ni}^{1+}\text{-CO}$ (top). ACS in the $D_{\text{red}}\text{Ni}^{2+}$ state can also bind $\text{CH}_3\text{-Co}^{3+}\text{FeSP}$, forming a complex (right). The methyl group is transferred, yielding a complex in the state $D_{\text{ox}}\text{Ni}^{2+}\text{-CH}_3$ and Co^{1+} (bottom). The two proteins dissociate, yielding a form of ACS (left) that can either react with substrates CO and CoA to form product or react with Ti^{3+} citrate or dithionite to form the inactive state $D_{\text{red}}\text{Ni}^{2+}\text{-CH}_3$ (far-left).

the methyl group transfer reaction in accordance with $K_d = 180 \pm 90 \mu\text{M}$. These relationships are summarized in Figure 6.

Kumar et al. have reported on this reaction previously, though only in the forward direction, only under one concentration of CO (added to the ACS syringe), and only under one set of protein concentrations.²⁰ Moreover, their analysis involved simply calculating an apparent first-order rate constant for the process. To compare our results to theirs, we used our four-step model and their initial concentrations to simulate their data. Then we determined the corresponding apparent first-order rate constant of the simulation. The value obtained, 3.2 s^{-1} , is ~ 2.5 times greater than that obtained by Kumar et al. (1.2 s^{-1}).

CO inhibits the synthesis of acetyl-CoA,¹⁷ and our study identifies methyl group transfer as the step (or at least one of the steps) in the catalytic mechanism responsible for this effect. CO inhibits by forming a nonproductive but reversible complex with ACS_{red} . Fits to steady-state kinetic plots of ACS-catalyzed acetyl-CoA synthesis in the presence of CO suggest that at least 3 CO's bind ACS, and that the binding is cooperative with $K_D \sim 0.9 \text{ mM}$ for the first CO binding step and $K_D \sim 50 \mu\text{M}$ for subsequent steps.¹⁷ The discrepancy between comparable parameters obtained from the two experiments ($50 \mu\text{M}$ vs $180 \mu\text{M}$) is not ideal, but given the complexity of the problem, the uncertainty of the determinations, and the different approaches used, we view these K_D values as generally congruent. Our inability to improve fits by adding additional CO binding steps suggests that CO binds ACS at other sites (and with other strengths) that are unrelated to methyl group transfer.

CO probably inhibits the reaction by binding to the site on ACS_{red} where the methyl group would otherwise bind (i.e. the Ni of the A-cluster). Alternatively, it may bind at a distant site that alters the electronic properties of the methyl-binding site. Both possibilities suggest an ordered catalytic mechanism in

which methyl group transfer precedes CO binding and CoA attack. Recent results suggest that the CO used for catalysis approaches the A-cluster via a proteinaceous tunnel originating at the CO/CO₂ redox active site, while the CO that inhibits acetyl-CoA synthesis binds to the A-cluster directly without migrating through the tunnel.¹⁷ The tunnel may control the sequence of events in the catalytic cycle and synchronize the two active sites, for example, by allowing CO to migrate only after the methyl group has bound.

The invariant rate at which the methyl group of $\text{CH}_3\text{-Co}^{3+}\text{-FeSP}$ transferred to ACS, independent of whether ACS had been reduced by dithionite or Ti^{3+} citrate, suggests that both reductants had sufficiently low reduction potentials and were added in sufficient amounts to reduce the D site fully. Both reductants have $E^0 \sim -0.5 \text{ V}$ vs NHE, consistent with $E^0_{D_{\text{ox}}/D_{\text{red}}}$ of -0.4 to -0.5 V .⁸

The ACS catalytic mechanism proposed by Barondeau and Lindahl requires that the D site remains oxidized in the $\text{CH}_3\text{-ACS}_{\text{ox}}$ and $\text{CH}_3\text{-C(O)-ACS}_{\text{ox}}$ states.⁸ If D were reduced in either state, it could not accommodate the electron pair generated during the last step of catalysis (a reductive elimination in which $\text{CH}_3\text{C(O)-ACS}_{\text{ox}}$ is attacked by the thiolate of CoA yielding $\text{CH}_3\text{C(O)-CoA} + \text{ACS}_{\text{red}}$). Our result that Ti^{3+} citrate and dithionite inhibit the reverse methyl group transfer reaction (when they were preincubated with $\text{CH}_3\text{-ACS}_{\text{ox}}$) is readily explained by assuming that these reductants reduced the D site of $\text{CH}_3\text{-ACS}_{\text{ox}}$. The rate of reduction by Ti^{3+} citrate appears to be slow relative to the rate of methyl transfer, as this reductant did not inhibit the reaction when exposed to $\text{CH}_3\text{-ACS}_{\text{ox}}$ at the time of mixing with $\text{Co}^{1+}\text{FeSP}$. In contrast, dithionite partially inhibited methyl group transfer under these conditions. We are uncertain whether dithionite reduces the D site faster than Ti^{3+} citrate does, or whether dithionite interacts with $\text{Co}^{1+}\text{FeSP}$ and inhibits its methylation. The latter possibility is supported by the need to remove dithionite from CoFeSP (by Sephadex G25 chromatography and subsequent oxidation with thionin) prior to methylation.⁸ These differences may relate to dithionite's ability to inhibit CO/acetyl-CoA exchange activity fully³⁷ and to Ti^{3+} citrate's ability to inhibit the synthase reaction only after some period.³⁸

We attempted to fit a single-step reaction to the forward and reverse methyl group transfer experimental traces, but fits were unsatisfactory. Satisfactory fits were obtained with a mechanism involving (a) binding of ACS_{red} to $\text{CH}_3\text{-Co}^{3+}\text{FeSP}$, (b) intracomplex methyl group transfer, and (c) dissociation of $\text{CH}_3\text{-ACS}_{\text{ox}}$ and $\text{Co}^{1+}\text{FeSP}$. Proteins in the pre-transfer $\{\text{CH}_3\text{-Co}^{3+}\text{FeSP}:\text{ACS}_{\text{red}}\}$ complex are bound slightly tighter ($K_D \sim 0.12 \pm 0.06 \mu\text{M}$) than those in the post-transfer $\{\text{Co}^{1+}\text{FeSP}:\text{CH}_3\text{-ACS}_{\text{ox}}\}$ complex ($K_D \sim 0.3 \pm 0.2 \mu\text{M}$). Moreover, our fits suggest that the rate at which the pre-transfer species bind is ~ 15 times faster than that at which the post-transfer species bind, and that the rate at which it dissociates is ~ 5 times that at which the postreaction complex dissociates. Thus, the pre-transfer complex is bound more tightly than the postreaction complex, but it dissociates and associates more rapidly. These K_D values are a few hundred times smaller (i.e. tighter) than the $K_D = 26 \mu\text{M}$ measured for dissociation of phen-ACS and CoFeSP. Some or all of this discrepancy may be due to the use

(37) Ragsdale, S. W.; Wood, H. G. *J. Biol. Chem.* **1985**, *260*, 3970–3977.

(38) Maynard, E. L.; Lindahl, P. A. *J. Am. Chem. Soc.* **1999**, *121*, 9221–9222.

of phen-ACS rather than native ACS.³⁹ The tight but “inert” post-transfer complex concept supports the proposal that ACS and CoFeSP remain complexed and in “synthase mode” until acetyl-CoA forms.³⁹

Our results indicate that the methyl group transfer reaction occurring within the protein complex is reversible with $K_{\text{eq}} \sim 2.3$. This value suggests that the nucleophilicity of the $\{\text{Ni}^{2+}\text{D}_{\text{red}}\}$ unit is comparable to that of a Co^{1+} cobalamin, a well-known potent nucleophile.⁴⁰ Reduction of the D-site appears to anoint the Ni^{2+} of the A-cluster with properties expected for the Ni of an organometallic Ni^0 complex.

The rates observed here are substantially faster than those of other reported methyl group transfer reactions. Methionine synthase is a cobalamin-containing enzyme that catalytically transfers the methyl group of methyltetrahydrofolate to homocysteine. In the first half-reaction, enzyme-bound homocysteine reacts with methylcobalamin, forming methionine and Cob(I)alamin. This transfer occurs in accordance with a second-order forward rate constant of $0.0023 \mu\text{M}^{-1} \text{s}^{-1}$.⁴¹ In the second half-reaction, CH_3 -THF binds and transfers its methyl group to Cob(I)alamin with the rate constant of $0.0006 \mu\text{M}^{-1} \text{s}^{-1}$. In

another system, Scovell reports the kinetics and mechanism by which the methyl group of methylcobalamin transfers to palladium(II).⁴² PdCl_4^{2-} and methylcobalamin rapidly form a complex using the 5,6-dimethylbenzimidazole nitrogen, and then the methyl group is slowly transferred, in accordance with $k = 7.7 \times 10^{-9} \mu\text{M}^{-1} \text{s}^{-1}$. In another example, the rate constant associated with the methyl group transfer from an organocobalt(III) complex to a nickel(I) complex was reported to be $0.00243 \mu\text{M}^{-1} \text{s}^{-1}$.²² The closest comparison to these values would be the apparent second-order rate constants obtained by fitting reaction 1 to the forward and reverse reaction data. The best-fit k_f for CoFeSP-to-ACS methyl group transfer ($\sim 7 \mu\text{M}^{-1} \text{s}^{-1}$) is 2900-times greater than that for the Co-to-Ni complex transfer, 3500–11700-times greater than that involving methionine synthase, and 10^9 -times faster than the methylcobalamin-to-Pd transfer! These rate differences highlight the unique catalytic capabilities of the $\{\text{ACS}:\text{CoFeSP}\}$ system in general and the $\{\text{A-cluster}:\text{D-site}\}$ unit in particular.

Acknowledgment. This work was supported by an NIH grant (GM46441). We thank Ernest L. Maynard and Gheorghe Maria for helpful discussion, and Qingwu Yang for help in formatting graphics.

JA016676R

(39) Maynard, E. L.; Lindahl, P. A. *Biochemistry* **2001**, *40*, 13262–13267.

(40) Banerjee, R. V.; *Chemistry and Biochemistry of B12*; Wiley-Interscience: New York, NY, 1999.

(41) Banerjee, R. V.; Frasca, V.; Ballou, D. P.; Matthews, R. G. *Biochemistry* **1990**, *29*, 11101–11109.

(42) Scovell, W. M. *J. Am. Chem. Soc.* **1974**, *96*, 3451–3455.